United States Department of Commerce
Technology Administration
National Institute of Standards and Technology

NISTIR 5043

Report No. 30
DYNAMOMETER-INDUCED RESIDUAL STRESS IN RAILROAD WHEELS: ULTRASONIC AND SAW CUT MEASUREMENTS

Raymond E. Schramm
Jacek Szelążek
Alfred V. Clark, Jr.

NISTIR 5043

Report No. 30
DYNAMOMETER-INDUCED RESIDUAL STRESS IN RAILROAD WHEELS: ULTRASONIC AND SAW CUT MEASUREMENTS

Raymond E. Schramm
Jacek Szelążek
Alfred V. Clark, Jr.

Materials Reliability Division
Materials Science and Engineering Laboratory
National Institute of Standards and Technology
Boulder, Colorado 80303

Prepared for
U.S. Department of Transportation
Federal Railroad Administration
Office of Research and Development
Washington, D.C. 20590

March 1995

U.S. DEPARTMENT OF COMMERCE, Ronald H. Brown, Secretary
TECHNOLOGY ADMINISTRATION, Mary L. Good, Under Secretary for Technology
NATIONAL INSTITUTE OF STANDARDS AND TECHNOLOGY, Arati Prabhakar, Director

CONTENTS

LIST OF SYMBOLS

Abbreviations

As-Man.	- As-Manufactured
Avg.	- Average
brf	- Back Rim Face
DE	- Destructive Evaluation
EMAT	- Electromagnetic-Acoustic Transducer
FRA	- Federal Railroad Administration
frf	- Front Rim Face
NDE	- Nondestructive Evaluation
NIST	- National Institute of Standards and Technology
PET	- Piezoelectric Transducer
SD	- Standard Deviation
TTC	- Transportation Technology Center, Association of American Railroads

Symbols

δ	- Flange Tip Opening Displacement
σ	- Stress

Units

hp	- horsepower	lb	- pound
in	- inch	MHz	- 10^{6} hertz
kN	- 1000 newtons	mm	- 10^{-3} meter
ksi	- 1000 pounds per square inch	MPa	- 10^{6} pascals
kW	- kilowatt	μm	- 10^{-6} meter

Residual Stress in Induction-Heated Railroad Wheels: Ultrasonic and Saw Cut Measurements

Raymond E. Schramm, Jacek Szelążek,* and Alfred V. Clark, Jr.

Materials Reliability Division
Materials Science and Engineering Laboratory
National Institute of Standards and Technology
Boulder, Colorado 80303-3328

This is Report Number 30 in a series covering research performed by the National Institute of Standards and Technology for the Federal Railroad Administration. This report covers a project by the Materials Reliability Division to develop and test an ultrasonic system for measuring residual stress in the rims of railroad wheels.

The effect of stress on elastic parameters causes a small change in sound wave velocity. This acoustoelastic effect is the basis for a method of nondestructive evaluation (NDE). We used two types of ultrasonic transducers, piezoelectric and electromagnetic, to measure both thickness-averaged and near-surface stresses in the rims of twenty unused, cast-steel railroad wheels. The manufacturer mounted these wheels on a unique dynamometer and induced thermal damage by dragging tread brakes to simulate in-service conditions that might generate tensile hoop stress. After our ultrasonic nondestructive tests, they cut eighteen wheels with a saw along a radius to measure flange tip opening and verify the stress state. The displacement of the opening (after cutting completely through the rim) indicates the net rim force. We correlated the ultrasonic measurements and the saw cut opening, showing that this approach may be useful for field assessment of wheel safety. Wheels with negative net rim force are in compression and will likely arrest any cracks. Wheels with positive rim force may suffer failure by crack propagation.

Key words: EMAT; nondestructive testing; piezoelectric; railroad wheel; residual stress; ultrasonic

* NIST Guest Researcher on leave from the Institute of Fundamental Technological Research, Polish Academy of Sciences, Warsaw

1. CONTRACT HISTORY

Our work to develop ultrasonic nondestructive evaluation methods for railroad wheels began in 1985. While the original emphasis was on roll-by detection of tread cracks, the emphasis has changed to include the measurement of residual hoop stress in the rims. Here, the goal is to develop a reliable, quantitative method that is useful in a wheel shop environment. This work was done under a three-year research contract, Reimbursable Agreement No. DTFR53-91-X-0068 with an effective date of May 30, 1991.

Since the last report, we have made oral presentations at technical meetings with published proceedings:

1. R.E. Schramm, A.V. Clark, and J. Szelążek, "Safety Assessment of Railroad Wheels by Residual Stress Measurements," in *Nondestructive Evaluation of Aging Railroads*, Donald E. Gray, Daniel Stone, Editors, Proc. SPIE 2458, 97-108 (1995).

2. R.E. Schramm, J. Szelążek, A.V. Clark, Jr., G. Garcia, and R.A. Pilon, "Railroad Wheel Rim Stresses: Ultrasonic Measurement to Guide Replacement-for-Cause," World Conference on Railway Research, Colorado Springs, CO, June 17-19, 1996 (to be published).

Prior reports in this series of National Institute of Standards and Technology Internal Reports (NISTIRs) have been:

1. R.E. Schramm and A.V. Clark, Jr., "Report No. 18 - Ultrasonic Railroad Wheel Inspection Using EMATs," NISTIR 88-3906, December 1988.

2. R.E. Schramm, A.V. Clark, Jr., D. V. Mitraković, Y. Cohen, P.J. Shull, and S.R. Schaps, "Report No. 22 - Tread Crack Detection in Railroad Wheels: An Ultrasonic System Using EMATs," NISTIR 3967, May 1991.

3. R.E. Schramm, A.V. Clark, Jr., D.V. Mitraković, S.R. Schaps, and T.J. McGuire, "Report No. 23 - Residual Stress Detection in Railroad Wheels: An Ultrasonic System Using EMATs," NISTIR 3968, May 1991.

4. R. E. Schramm, J. Szelążek, and A.V. Clark, Jr., "Report No. 28 - Residual Stress in Induction-Heated Railroad Wheels: Ultrasonic and Saw Cut Measurements," NISTIR 5038, May 1995.

2. INTRODUCTION

Inspection of railroad wheels during their service life and replacement when necessary is an important element of safe operation. This is an expensive process [1]. One problem is wheel condemnation before normal wear-out due to tensile residual stress developed around the rim during thermal abuse from severe drag-braking. Such stress may drive crack growth [2], so safety requires finding and removing damaged wheels; economy seeks removal only when necessary. The study of this problem has generated considerable international cooperation [3] and constant improvements in wheel geometry [4].

Until 1995, a Federal Railroad Administration (FRA) regulation required wheel replacement whenever a band of heating discoloration extended 100 mm (4 in) or more into the plate area [5]. Unfortunately, about half the condemned wheels were still in rim compression [6-8], a safe condition in which the wheels are manufactured. Even worse, some wheels with unsafe tension did not show discoloration to this extent. An efficient and reliable method of quantitative nondestructive evaluation (NDE) would contribute to both safety and economy.

Some NDE methods available include x-ray [9] and neutron [10] diffraction, magnetic [11] and Barkhausen [12-14] effects, and combinations such as the magnetoacoustic effect [15]. The hole-drilling approach [16] is minimally destructive. Both diffraction methods present radiation hazards. In addition, a nuclear reactor is required to supply the required neutron intensity, and x-rays give information on only a very thin surface layer. The magnetic effects, including Barkhausen, are very sensitive to material composition and metallurgical condition. The magnetoacoustic effect has a high detection threshold. Hole drilling, like all these other methods, demands a very skilled operator and considerable time. None of these tools seem to be likely candidates for routine use in a maintenance-shop environment.

Ultrasonic velocity varies slightly with the stress state of the supporting medium. This acoustoelastic effect [17-21] offers the possibility of probing the bulk of the wheel rim with compact gear and without radiation problems. Automation could make the measurement rapid and routine. This program has explored this possibility.

This investigation employed two different types of ultrasonic transducers:

1. Electromagnetic-acoustic transducers (EMATs) in a system developed at NIST. This uses polarized shear waves to measure thickness-averaged stress;

2. More conventional piezoelectric transducers (PETs) that were part of a portable stress instrument developed by the Institute of Fundamental Technological Research of the

Polish Academy of Sciences. This instrument measured stress as above and also used near-surface signals to test stress levels there.

The most obvious distinction for a user is that EMATs do not require the fluid acoustic couplant required by PETs.

In cooperation with the Transportation Technology Center (TTC) of the Association of American Railroads (AAR) in Pueblo, Colorado, the major wheel manufacturer for U.S. freight cars has provided us with unused wheel specimens containing controlled levels of thermal damage. For a baseline, we also looked at as-manufactured wheels. In our last report [22-23], the thermal damage was the result of inductive heating at the tread. In this report, the wheels were drag-braked on a special dynamometer built by the manufacturer to simulate in-service conditions more closely.

Following our extensive NDE measurements, the manufacturer made destructive evaluation (DE) measurements by cutting 18 of the wheels along a radius. The degree and direction of the opening displacement (measured by a strain gage on the tip of the flange) indicated the forces in the rim. As in prior work cited above, this was necessary to validate the ultrasonic methods.

3. SPECIMENS

As in our previous work, all the test wheels were unused, cast steel, with a nominal diameter of 910 mm (36 in). They were single wear, curved plate, and heat treated (CH36, class C). While all the wheels examined here were from the same plant, they did come from several production runs.

This style of wheel has 10 casting risers that are cut off and ground down, but their location was still visible on the front plate. We used these as landmarks for the multiple measurements around the circumference. We numbered these risers sequentially 1 through 10 and made measurements on the rim face at these locations. We made an additional 10 measurements half way between each pair of risers.

Metallographically, there are roughly two regions in the cross section on the rim (Fig. 1). An outer layer with a thickness of about 20 mm consists of dendritic grains oriented perpendicular to the surface. An inner region contains small, randomly oriented grains. This texture is the result of cooling and solidifying in the graphite mold. Most of the wheels used in Europe are

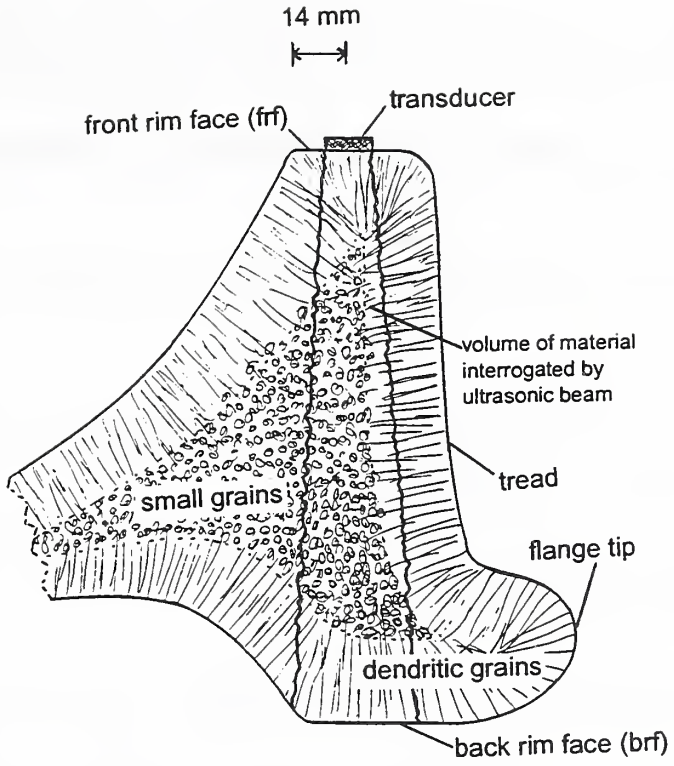

Fig. 1. Schematic of the cross section of a cast-steel wheel rim. Compare to the photographs in Figs. 19-20 of reference 24. The outer grains are dendritic and normal to the surface. At the interior, the grains are mostly small with random orientation.

forged and machined [25] and this generally yields a uniform, small grain structure; in some cases, there is no obvious texture.

4. DYNAMOMETER BRAKING

The wheel manufacturer's dynamometer has a unique configuration with two standard wheel trucks, each having one axle mounted with a pair of wheels. The first truck has a permanently mounted axle connected to the drive motor. The wheels on this axle have a profile ground to the same shape as a standard rail. The axle in the second truck holds the test wheels. This system exerts a normal load between trucks to simulate the loading seen in service.

For all wheels, the damage procedure was:

1. An initial conditioning of three pairs of brake shoes. This was a 34 kW (45 hp), 30-min run with each pair. This smooths the shoe surface without tread damage.

2. Three damage runs (changing brake shoes between) at the rated power and shoe position.

3. Between runs, air-cool the wheels to at least 260° C (500° F) and then water-cool.

There were several parameters for these damage runs:

1. Brake shoe position: centered on the tread (properly aligned), or crowding the flange (simulating one type of misalignment).

2. Normal load between opposing trucks. Here it was about 111 kN (25,000 lb), or about 2/3 of the maximum seen in service.

3. Equivalent speed. Usually, it was 97 km/h (60 mph).

4. Loading on the brake shoes. When the shoes were centered on the tread, this loading was normal to the tread. During the flange-crowding tests, the load had an additional tangential component. These loads and the drive speed (#3) were the main components in calculating the energy input to the wheel tread.

5. Time of run:

    a. For the first sixteen wheels (least damage), the session ran for 30 min with each of the three sets of shoes.

    b. For the last four wheels (greatest damage), each of three sessions per wheelset ran until the shoes disintegrated (about 55 min).

Table I summarizes the dynamometer runs on 20 specimens.

Thermocouples riding on the tread measured the temperature. Pyrometer (infrared) measurements were also made at several radial positions in the wheels plate. Some localized hot spots became apparent by visible radiation, but local increases in stress were not evident.

Table I. Summary of 20 specimens run on dynamometer.

Dynamometer runs	Power, kW (hp) (shoe position)	Number
3 × 30 min	56 (75) (flange)	2
	60 (80) (flange/center)	4
	63 (85) (flange/center)	4
	67 (90) (flange/center)	4
	75 (100) (center)	2
3 × shoe wearout	63 (85) (flange/center)	4

Figure 2 is a sample of the tread temperature data collected by the manufacturer for a pair of 60 kW specimens. For 75 kW power, the maximum wheel temperature was about 50 to 60° C higher, while the rail temperature remained about the same.

In an earlier part of this program on induction-heated wheels [23], the energy transfer efficiency was likely very close to 100%. In previous work on wheels damaged on a standard dynamometer (direct drive of the test wheel, tread contact only with the brake shoe) [26], the efficiency was estimated at 2/3. In this machine, tread contact with the drive wheels absorbs some heat energy from the tread (due to continuing contact, the simulated rail became much hotter than a real rail would). By comparing saw-cut openings from induction-heated wheels and those damaged on this new dynamometer, the manufacturer estimates the energy transfer into the specimen to be about 56%. Because of these differences in efficiency, we cannot directly compare induced damage between these various mechanisms. In-service conditions can also vary widely (wind, rain, brake shoe position, etc.).

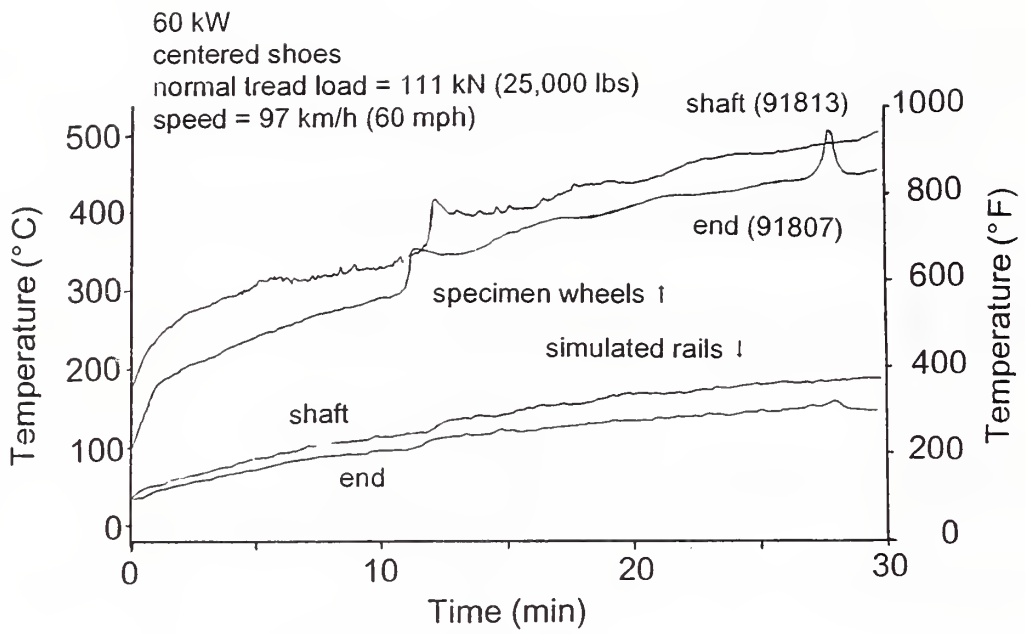

Fig. 2. Typical record of wheel and rail tread temperatures during one 30 min run.

5. ULTRASONIC STRESS MEASUREMENT

5.1 Principles

Previous reports have documented most of the theory and application of the acoustoelastic theory to stress measurement [22-23]. Any stress field influences the velocity of a sound wave passing through it, depending on its mode and polarization. While the effect is small (parts in 10^4), it is possible to measure it routinely with the proper equipment and care. Unfortunately, any metallurgical texture present may influence the velocity to the same degree. The challenge is to separate these effects in a way that will give reliable stress measurements.

The principal method used in this study used shear-horizontal (SH) waves introduced into the front rim face of the railroad wheel. The waves traveled through the rim thickness and reflected from the back rim face to return to the transducer. By comparing the travel time, a measure of velocity, for radial and circumferential (or hoop) polarizations (birefringence), we can calculate the difference in stress for these two directions. Of the two, the radial stress is likely to be much smaller, so the result is a measure of the hoop stress present in the wheel rim. The calculated stress is the average through the thickness.

A secondary method combined both shear and longitudinal waves traveling along the front and back rim faces. Using both wave types minimized the effect of texture. By comparing with a reference specimen (usually stress relieved), it is possible to measure the hoop stress near the surface. There were four sets of transducers (one transmitter and two receivers); travel times for both types of waves were measured in opposing directions to average out the effects of surface roughness.

To try to eliminate the influence of texture in the cast steel wheels, we made many measurements on small blocks (200 mm long) cut from the rims of new and used wheels of the same type. The cutting removed most of the mechanical restraints to relieve any stress, and heat treatment [23] reduced stress to a minimum. The resultant specimens should display only texture effects. These measurements indicate variability and the kind of accuracy possible if we applied an average value to our test wheels.

Another approach to this texture problem is to collect statistically significant data on new, unused wheels (with their designed compressive stress). Our limited experience suggests that the stress and texture are both fairly repeatable. Measurements from in-service wheels would then indicate any change from this safe state.

5.2 Equipment

While the underlying physics is the same, there were two distinct systems in this study to generate and detect ultrasonic waves:

1. A piezoelectric transducer (PET). This device underlies the more conventional approach to ultrasonic studies. A small section of piezoelectric material is electrically shocked into mechanical resonance. The vibrations pass through a face plate and fluid couplant into the specimen. The return signal reverses this process.

2. An electromagnetic-acoustic transducer (EMAT). This device is becoming more common with increasing availability of compatible electronics. It contains a wire coil and a magnet. A radio-frequency electrical pulse through the coil generates an eddy current in the specimen surface; this interacts with the magnetic field to produce the mechanical vibrations of sound.

The PET system used here is commercially available [27]. The EMAT system was built at NIST, although commercial versions are also available [28, 29]. Most of the measurements here used shear horizontal waves traveling through the rim thickness (giving the thickness-averaged stress). This operation used the pulse-echo method, one transducer being used for transmitting

and receiving. The PET system also had a special probe containing 12 transducers (operated pitch-catch) that sent waves along the surface of the rim face. This method used both longitudinal and shear waves to measure near-surface stresses.

For the shear-wave PET transducer used to measure thickness-averaged stress, the couplant was a thick epoxy resin, viscous enough to support shear waves. For the surface probe, the shear waves were generated by mode-conversion at the transducer-specimen interface; this system used both longitudinal and shear waves refracted to travel along the surface. In this case, a water-based gel proved to be a good couplant.

The required precision in measuring the signal arrival time was a few nanoseconds. (The round-trip time for a shear wave through the rim thickness was about 90 μs.) In the PET system, a marker was manually placed on the first peak of the signal. In the EMAT system, an electronic gate marked the zero-crossing of a selected cycle in the signal. For the thickness-averaged measurements, the PET used the time difference between first and second echoes to minimize any influence of variations in the thickness of the fluid couplant and surface roughness. The EMAT measured the arrival time of only the first echo. Both systems operated at about 2 MHz.

In all cases, the center of the transducer was at the midpoint of the front rim face (frf), 14 mm from the inside edge. The EMAT system had an apparatus to find this edge and position the transducer.

Both systems have their own advantages and disadvantages. Among these are:

1. The PET requires more operator involvement in setting the timing mark, while the EMAT needs some attention to maintain the gate setting on the proper cycle. The PET requires physical rotation of the transducer, while the EMAT has a dual coil to avoid this. (Both systems are undergoing upgrades that will reduce most of this operator involvement [20].)

2. The PET uses more readily available electronics and generates a stronger signal. The EMAT requires more specialized electronics and the signal is much weaker.

3. The PET needs an acoustic couplant which takes operator time and introduces uncertainties in timing measurements due to any variations in the thickness of this couplant. The EMAT eliminates this step.

Figure 3 shows the two systems used in this work.

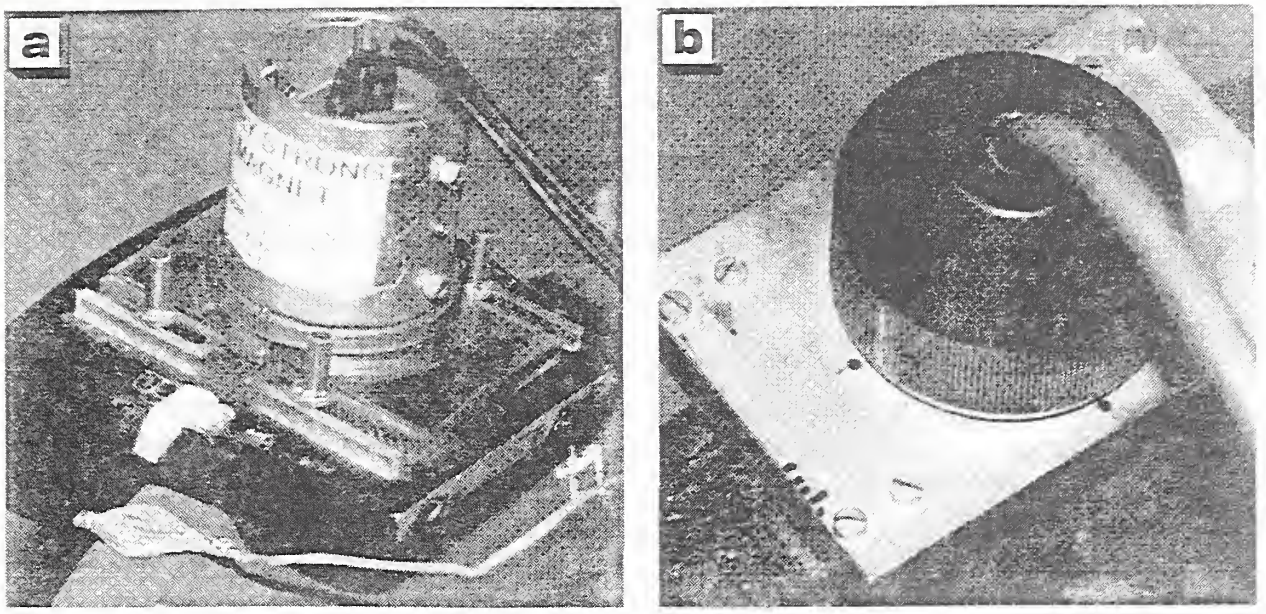

Fig. 3. Ultrasonic systems used to measured thickness-averaged stress in the rim of railroad wheels. The probes are on the front rim face.
a. EMAT in a fixture that establishes radial position.
b. PET; the probe to measure near-surface stress is longer.

6. NONDESTRUCTIVE MEASUREMENTS

6.1 Procedures

This program involved a large number of stress measurements at several points during the dynamometer procedures, and some duplicate measurements to examine repeatability. Such a quantity of data in this detail is possible only with relatively fast and easy NDE methods. At the manufacturer's site, before and during dynamometer runs, we made two or three pairs of measurements (on-riser and between-risers) around the circumference of most of the wheels. With EMAT and PET systems we checked thickness-averaged and surface stresses on the frf as well as surface stress on the back rim face (brf):

1. In the as-manufactured condition, before any damage.

2. On the dynamometer, after each brake shoe conditioning run (which introduced no stress).

3. On the dynamometer, after the first two damage runs.

After the final (third) dynamometer run, the wheels were dismounted from the axle and 16 were shipped to our laboratory. At this point we made measurements at 20 circumferential positions.

The last four wheels (parameter 5b of Section 4) were damaged at a later time and to a level where the possibility of wheel explosion precluded shipment. The measurements before and after dynamometer runs were made at the manufacturer's site (using only the EMAT system) by Greg Garcia of the Transportation Technology Center, Association of American Railroads, Pueblo, Colorado.

Each pair of wheels was identified by axle end when mounted on the dynamometer: the end nearest the drive motor shaft or the other, free end. Looking for systematic differences in the results from each pair of wheels on the same axle would reveal any misalignment problems in the drive shaft-axle system or the specimen and drive wheel trucks. We found no apparent difference among the pairs, suggesting good dynamometer alignment.

6.2 Thickness-Averaged Stress

Time constrictions limited the amount of data collected before and during the series of dynamometer runs. Figure 4 shows the stress measured on one pair of wheels with both ultrasonic systems. The abscissa is the circumferential position identified by the numbered casting risers (the beginning and end of the plot represent the same point). Figure 4a shows the as-manufactured state, before any damage. Figure 4b shows the same wheels after the initial, low power dynamometer runs to break in (condition) three pairs of brake shoes. These data are typical of our measurements, and reveal some common factors:

1. The stresses appear to be fairly uniform around the circumference.

2. The total spread of measurements is usually less than 50 MPa.

3. The hoop stress is compressive, as intended by the manufacturer.

4. As anticipated by the manufacturer, the low power of 34 kW used for shoe break-in does not alter the stress in the rim.

The limited measurements we made between the three damage runs showed that a single dynamometer session would generate most of the stress seen after all three runs. The second and third braking sessions served mainly to homogenize the stress around the circumference.

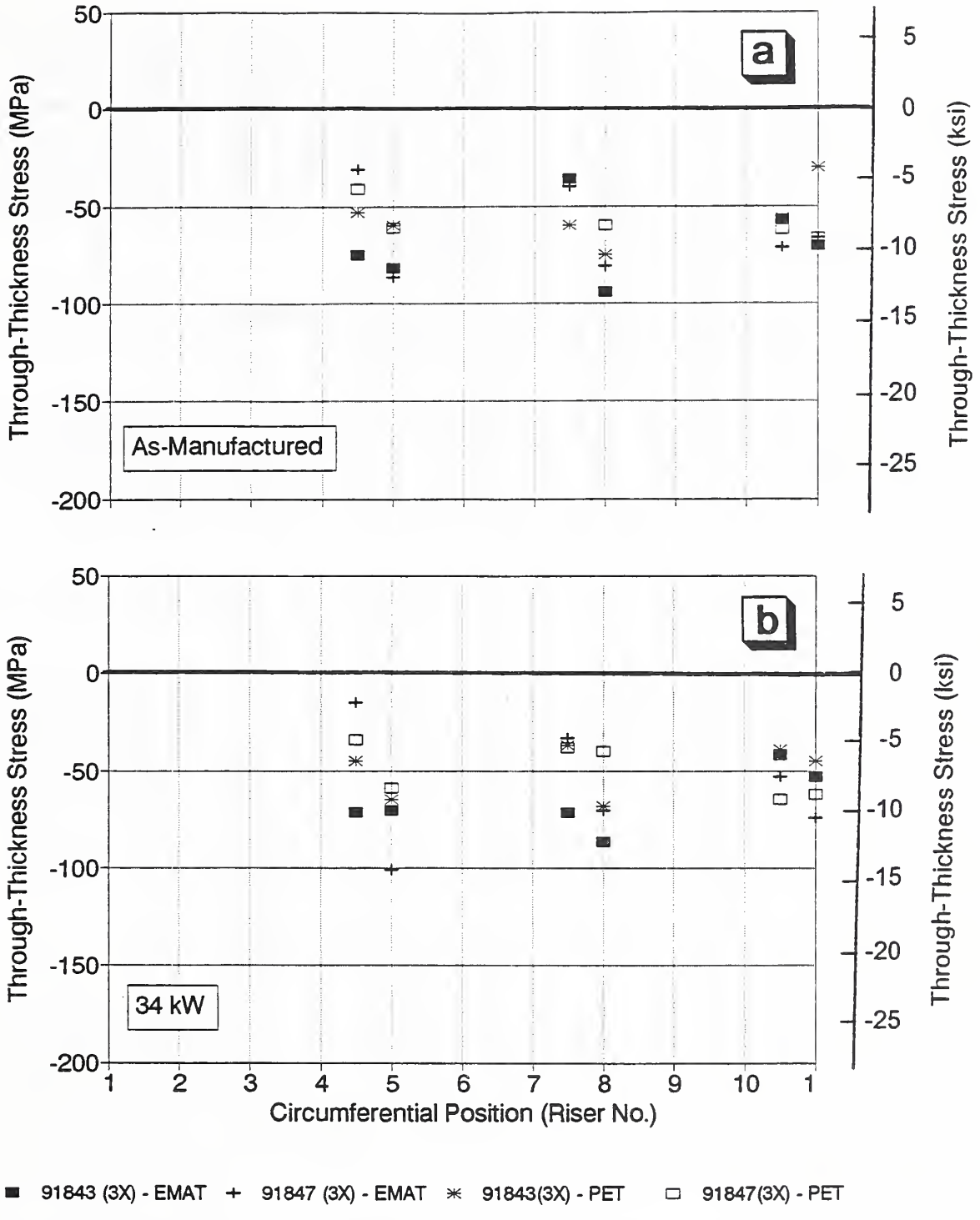

Fig. 4. Preliminary measurements (all from the frf) of thickness-averaged stress in one pair of wheels.

a. As-manufactured, prior to any damage

b. After break-in of three pairs of brake shoes (3 × 30 min at 34 kW)

After the dynamometer runs, the wheels were delivered to our laboratory and the luxury of time permitted detailed measurements around the entire circumference. Figure 5 shows 20 through-thickness stress measurements, one at each of the 10 casting risers, and between each pair. These data compare frf results from both EMAT and PET, as well as a frf/brf comparison for the EMAT. These are typical of the stresses we measured on all 20 wheels. While Fig. 5a is for a low power and Fig. 5b is for a high power, they were both measured after the full set of three 30 min runs. Some observations include:

1. There are stress variations around the circumference. Some of this may be due to texture, but prior work [23] showed stress variations also can exist.

2. There is a systematic offset between EMAT and PET data. As before [23], the PET results are generally higher, usually 40 MPa or less. This is likely due in large part to initial calibration measurements of the texture effect. It is possible that the different transduction mechanisms lead to differences in beam spread through the rim.

3. The EMAT and PET values do track each other very well, giving high confidence in their relative accuracy.

4. The brf values from the EMAT run consistently higher than the frf values. This is likely the result of seeing a different geometry as the beam spreads while traveling in opposite directions. (There were no brf PET values to compare.) The choice of rim face is likely to be a matter of convenience in the field. The frf would normally be most accessible.

5. The stress after 56 kW (Fig. 5a) was about equal to the as-manufactured condition.

6. The stress after 75 kW (Fig. 5b) has reversed and become slightly tensile.

For the last four wheels, the damage run for each of the three sets of brake shoes lasted until the brake disintegrated (approximately 55 min). As noted above, TTC personnel recorded these measurements at the dynamometer site. Figure 6 shows a typical data set. Three sets of measurements around the circumference showed excellent repeatability. Note that the stress level here was much higher than seen in Fig. 5b. During the saw cutting, this wheel exploded before the cut depth reached 76 mm (3 in).

Table II summarizes the through-thickness average hoop stress measured in the rims of all twenty wheels. These values represent the average of all measurements around the circumference. For the as-manufactured wheels, there were four or six measurements (two or three pairs), while there were twenty measurements after completion of damage.

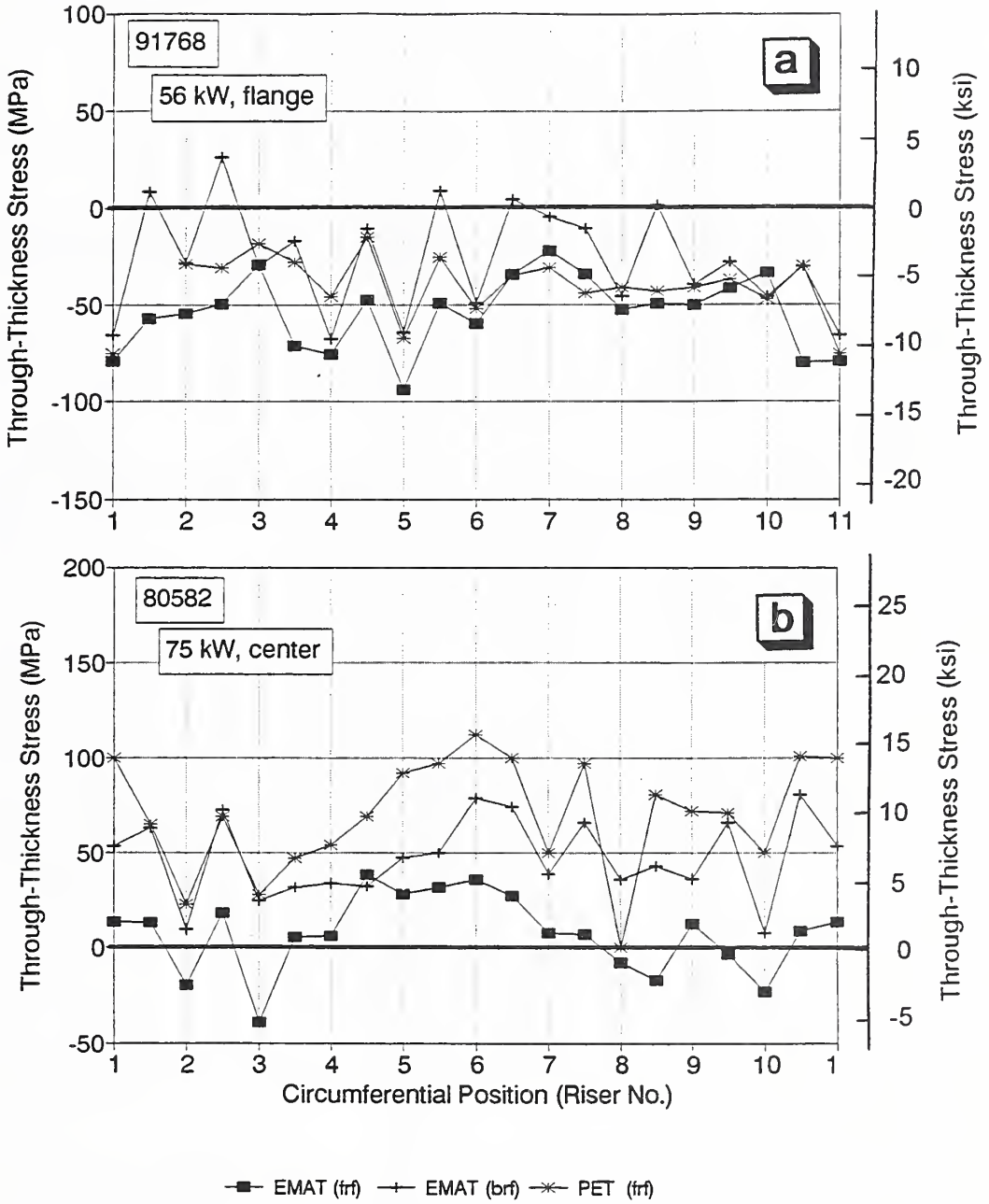

Fig. 5. Thickness-averaged stress around the entire circumference. The measurements include those taken with the transducer on the frf (both EMAT and PET) and on the brf (EMAT).

a. This wheel received 56 kW with the brake shoe crowded into the flange.

b. This wheel received 75 kW with the brake shoe centered on the tread.

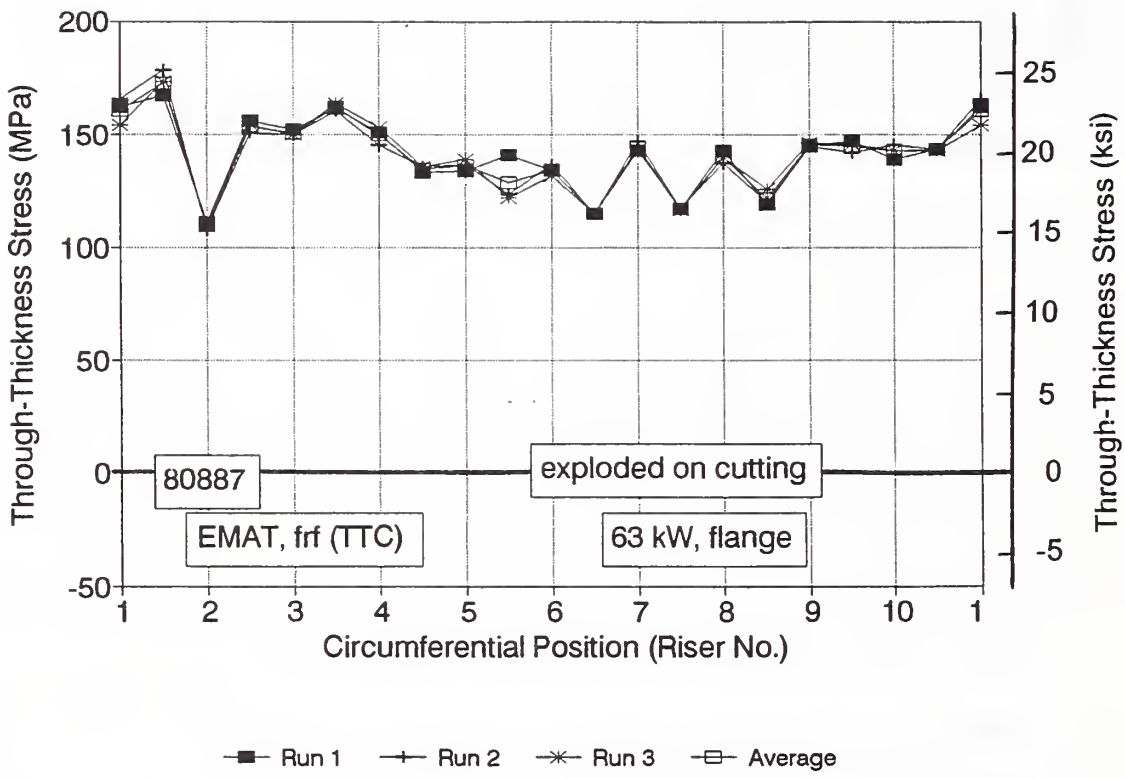

Fig. 6. Measurements on a wheel with high stress generated by running the dynamometer until shoe disintegration. Only the EMAT system was available for measurement by TTC personnel. During the destructive saw cutting, this wheel exploded due to residual stress.

Table II. Summary of through-thickness stresses measured from the frf with two ultrasonic systems on wheels as-manufactured and after braking.

Wheel ID	As - man. Avg.[a] σ (MPa) EMAT	As - man. Avg.[a] σ (MPa) PET	Braked Shoe position	Braked Power (kW)	Braked Avg.[b] σ (MPa) EMAT	Braked Avg.[b] σ (MPa) PET
91817[c]			flange[e]	56	-40	-13
91768[d]			flange[e]	56	-53	-39
91813[c]	-83		center[e]	60	-80	-11
91847[d]	-68		center[e]	60	-45	-15
84967[c]	-49	-31	flange[e]	60	-25	+6
91778[d]	-68	-53	flange[e]	60	-36	-22
91777[c]	-43	-56	center[e]	63	-37	-12
91784[d]	-71	-62	center[e]	63	-74	-37
91843[c]	-69	-56	flange[e]	63	-51	-18
91847[d]	-62	-55	flange[e]	63	-36	-13
76933[c]			center[e]	67	+4	+29
76896[d]			center[e]	67	+13	+54
63764[c]			flange[e]	67	-19	+1
83991[d]			flange[e]	67	-25	-13
80742[c]	-70		center[e]	75	-17	+23
80582[d]	-49		center[e]	75	+7	+74
84758[c]	-33	-28	center[f]	63	+11	
84972[d]	-19	-7	center[e]	63	+53	
86398[c]	-23		flange[f]	63	+64	
80887[d]	-63		flange[f]	63	+140	

Notes: Averages are around the circumference. [a] 4-6 measurements. [b] 20 measurements. [c] Shaft end of axle. [d] Free end of axle. [e] 3 × 30 min runs. [f] 3 × shoe wearout.

6.3 Surface Stress

The PET probe for near-surface stresses has a gage length of nearly 200 mm. Averaging the travel time over this distance effectively smooths local variations in stress or texture. The graphs in Fig. 7 show a relatively uniform stress around the circumference.

As with the inductively heated wheels [23], the stresses on frf and brf changed in opposite directions during the dynamometer runs. In Fig. 7a, the frf and brf stresses are both compressive and not very different from the as-manufactured case. After damage at 63 kW, a level that introduces only moderate damage as determined by the through-thickness stress (Table II), Fig. 7b shows the stress difference between the two faces has increased notably. While the brf stress became less compressive, the frf stress became more so. This again indicates that the thermal stresses have created an out of plane bending.

Table III summarizes the surface stresses measured on 18 of the 20 test wheels. These are the averages from the frf and brf measured before and after the dynamometer damage.

6.4 Precision

In Fig. 8, showing the spread in data for the through-thickness measurements, each vertical bar represents one wheel and shows the spread of stresses measured around the circumference. For the as-manufactured and 34 kW conditions, this included four or six measurements; for the others, there were twenty measurements. The horizontal tick shows the average. Within each energy category, we would expect similar values. Figure 9 shows the average and spread of the averages (ticks, listed in Table II) of the data in Fig. 8.

Several factors could contribute to uncertainties in calculated stresses from acoustic birefringence (thickness averaged). Some of them are:

Accuracy:

1. Value of the acoustoelastic constant.

2. Timing accuracy.

3. Stress distribution through the rim.

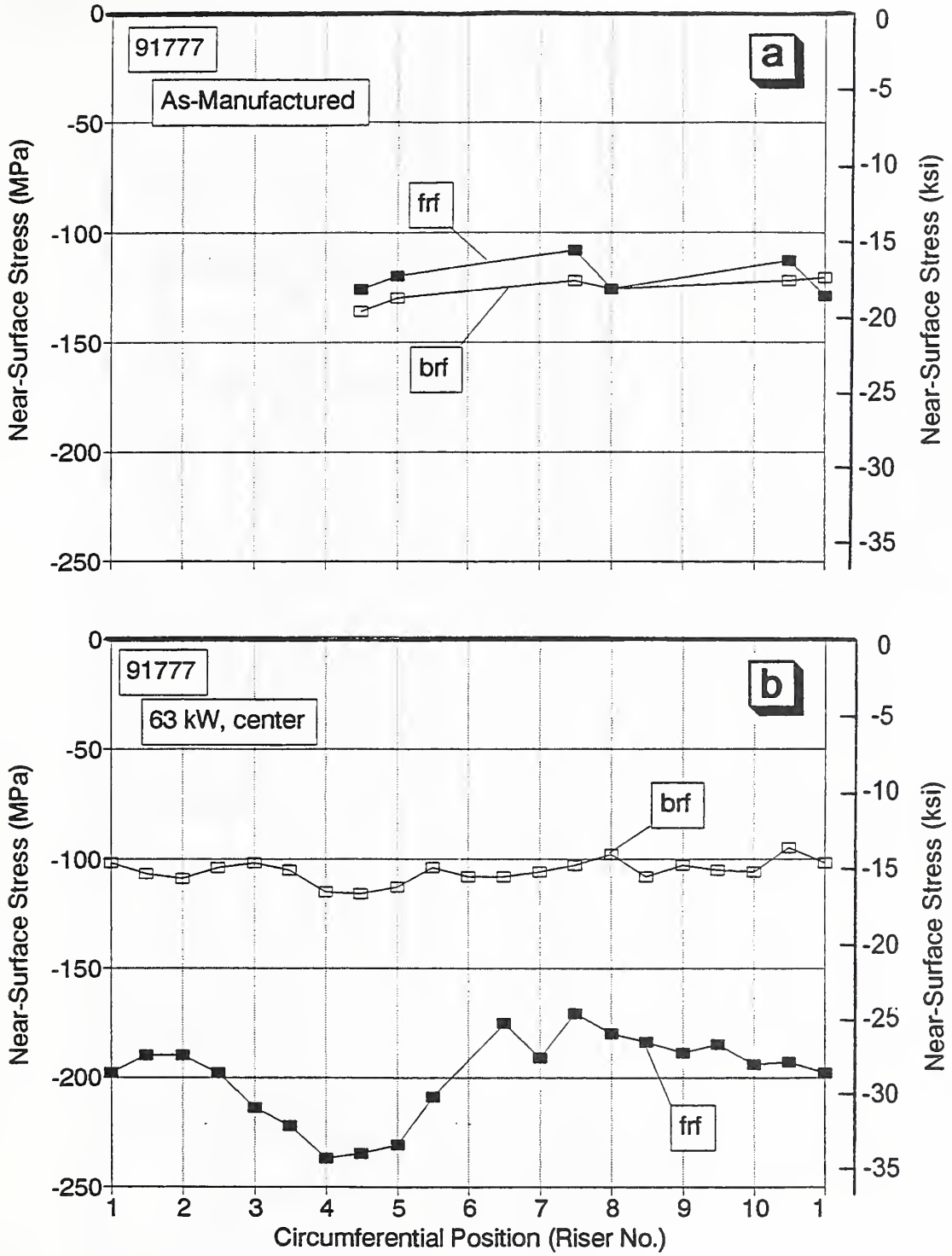

Fig. 7. Surface stresses measured around the circumference with the PET. a. As-manufactured. b. After 63 kW on the dynamometer.

Table III. Summary of near-surface stresses measured with the PET system on both rim faces of wheels as-manufactured and after braking.

Wheel ID	As - man.		Braked			
	Avg.[a] σ (MPa)		Shoe Position	Power (kW)	Avg.[b] σ (MPa)	
	frf	brf			frf	brf
91817[c]			flange[e]	56	-132	-99
91768[d]			flange[e]	56	-133	-129
91813[c]			center[f]	60	-171	-108
91807[d]			center[f]	60	-151	-92
84967[c]	-120	-120	flange[e]	60	-146	-108
91778[d]	-114	-110	flange[e]	60	-159	-98
91777[c]	-120	-129	center[e]	63	-189	-106
91784[d]	-148	-129	center[e]	63	-201	-114
91843[c]	-121	-120	flange[e]	63	-151	-100
91847[d]	-104	-127	flange[e]	63	-141	-101
76933[c]			center[e]	67	-235	-81
76896[d]			center[e]	67	-227	-71
63764[c]			flange[e]	67	-153	-85
83991[d]			flange[e]	60	-191	-101
80742[c]			center[e]	75	-213	-71
80582[d]			center[e]	75	-247	-85
84758[c]	-118	-101	center[f]	63		
84972[d]	-118	-112	center[f]	63		
86398[c]			flange[f]	63		
80887[d]			flange[f]	63		

Notes: Averages are around the circumference. [a] 4-6 measurements. [b] 20 measurements. [c] Shaft end of axle. [d] Free end of axle. [e] 3 × 30 min runs. [f] 3 × shoe wearout.

a.

b.

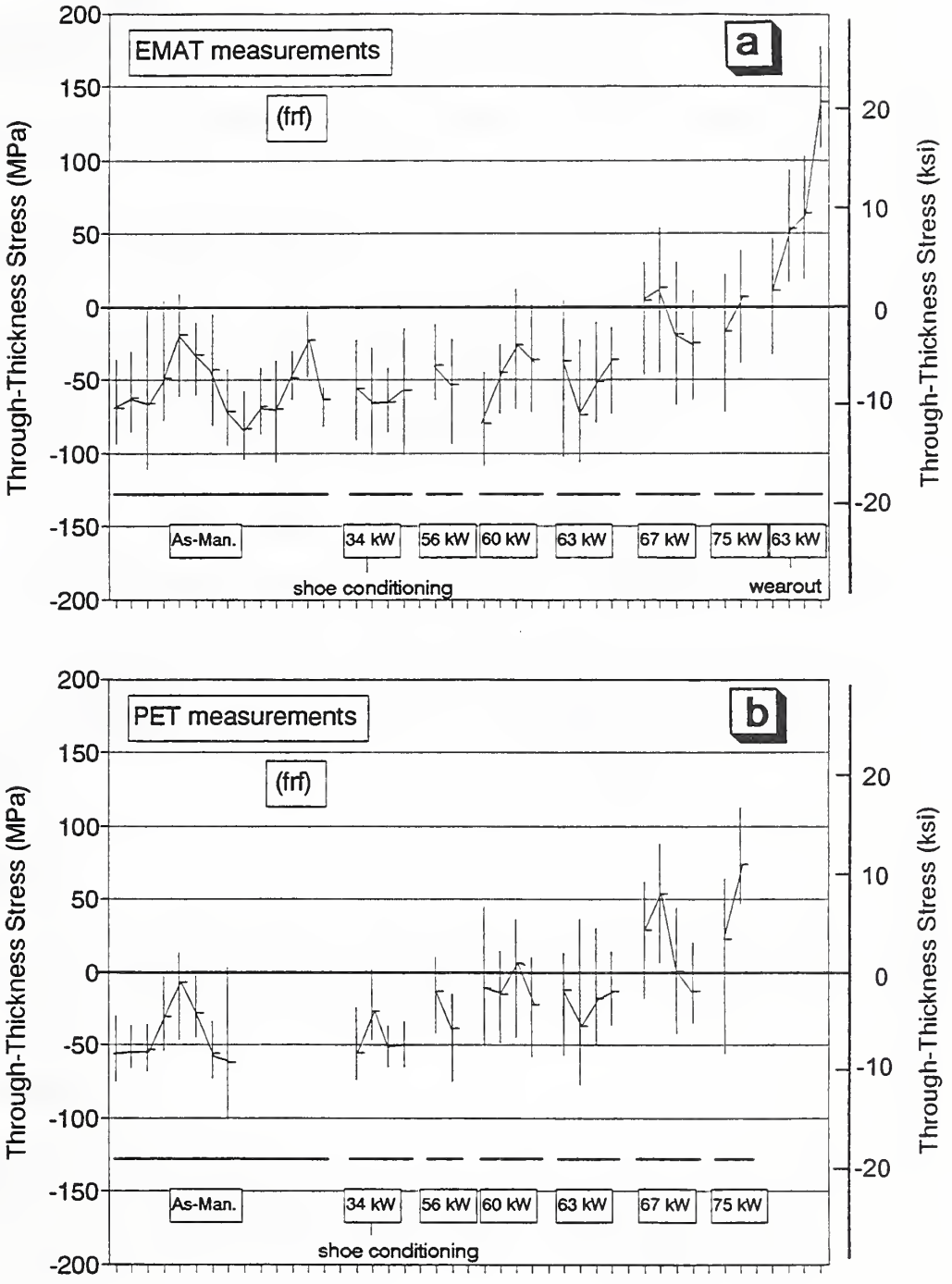

Fig. 8. Spread of through-thickness stresses measured on the frf. Each vertical line represents the range for one wheel. The tick on each line shows the average around the circumference. The horizontal bars indicate the power group.
a. EMAT measurements. b. PET measurements.

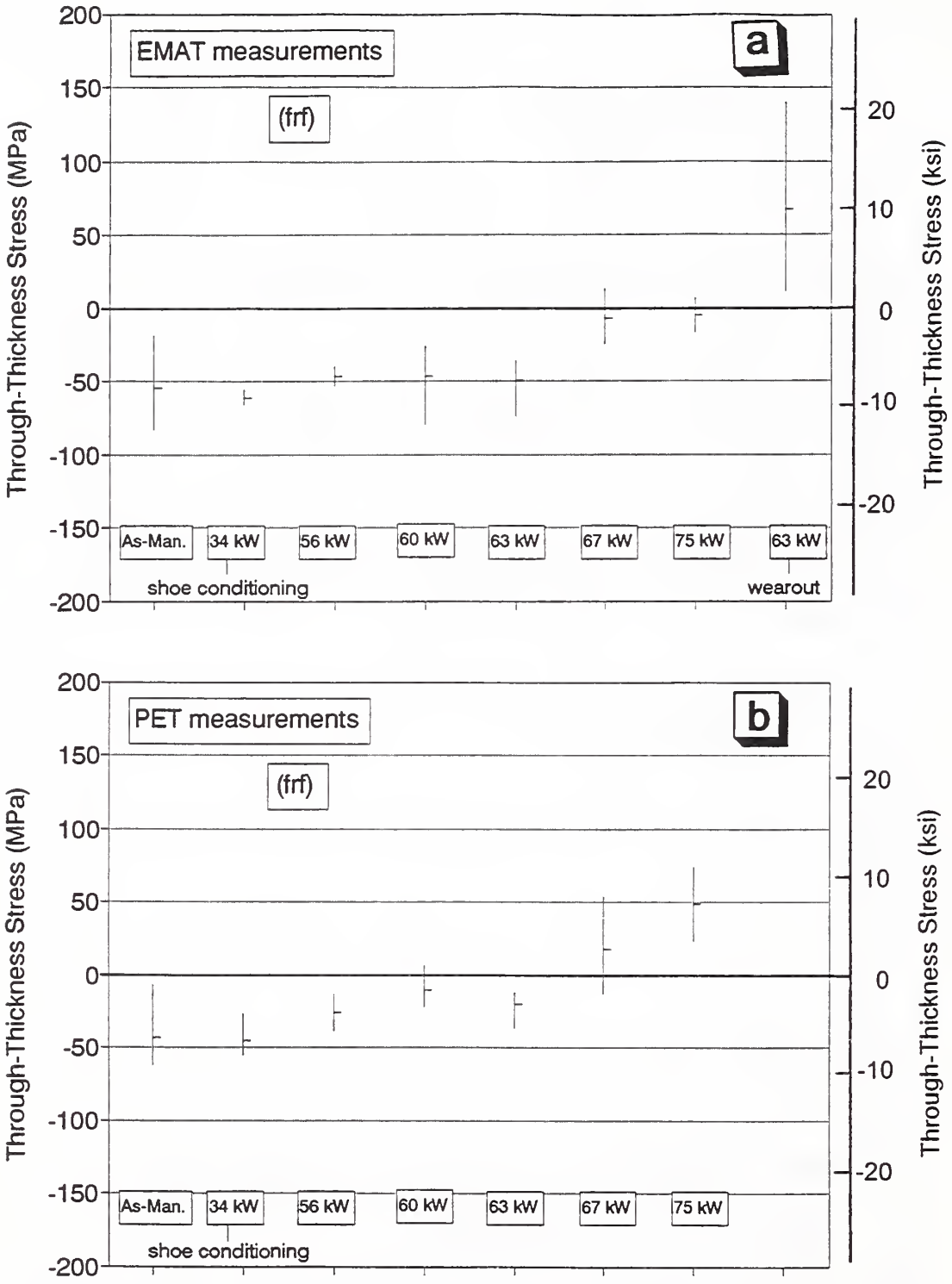

Fig. 9. Spread of the averages shown in Fig. 8 for each power group. The vertical line shows the total range of the averages, and the tick is the average of the averages. a. EMAT measurements. b. PET measurements.

Repeatability:

1. Radial position of transducer (accuracy of placement).

2. Transducer coupling to specimen (liftoff for EMAT and fluid thickness/uniformity for PET).

3. Variability of metallurgical texture.

While this list is not exhaustive, it probably does cover the major factors. At this point, the texture presents the greatest challenge. To get some handle on the size of this problem, we made a few series of measurements that should yield identical stress results within the group. The degree of variation in the calculated stress indicated our precision.

Rim Blocks

Seven rim blocks (one as-manufactured and two each from three induction-heated wheels) were cut from wheels from the same production run. Each block contained approximately 20% of the rim circumference. The plate was cut off and the block was heat-treated for stress relief. We calculated the stress from birefringence measurements near the two free ends. Since the stress should be essentially zero, any variations are due to texture variations among wheels.

As-Manufactured

Stress at two or three pairs (on-riser and between-riser) of points was measured on eight as-manufactured wheels at the producer's site. While these wheels were from two or three runs, they represent a production product with a relatively constant level of compressive stress.

Circumferential Details

After the damage runs on the dynamometer, we measured stress on eight wheels at several (9 to 19) points over a short (120 to 360 mm) portion of the circumference (Fig. 10). For each wheel, the rim stress should be nearly constant over this short distance, if not for texture variability.

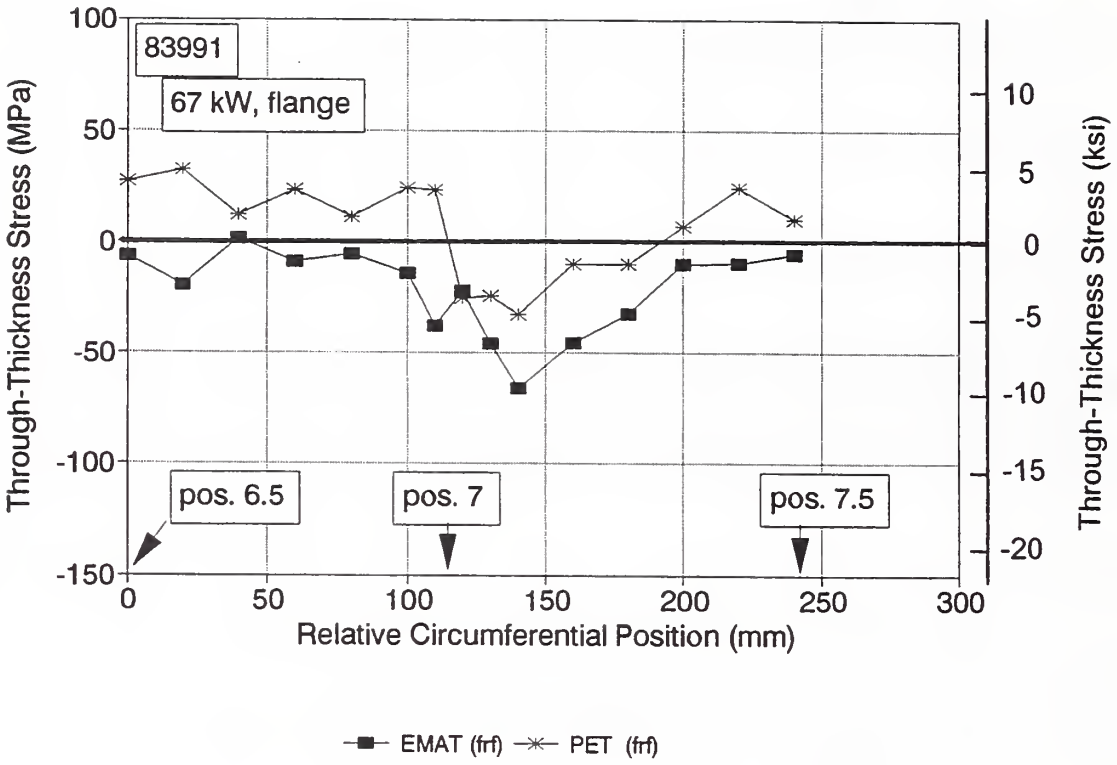

Fig. 10. Example of detailed measurements made over a short section of one wheel rim. Within this short distance, we would expect the stress to be nearly constant, so variations are likely due to texture. While the EMAT and PET measurements have an offset, as seen above, they track very well, even with this detail.

Table IV shows the average spread [spread = extent (maximum - minimum) of stress as measured at individual points in each specimen in the category. The average was calculated from all the spread values (Fig. 8)].

Table V shows the range of averages [the average was calculated for each specimen from all the measured points. Range = extent (maximum - minimum) of the average stress within each category (Fig. 9). Since the dynamometer wheels had received varying powers, their stresses would likely vary.]

Table IV. Through-thickness average spread.

Specimen category	Stress (SD) (MPa) EMAT	PET
Rim blocks	75 (±23)	102 (±33)
As-manufactured	58 (±22)	50 (±24)
Details	64 (±9)	68 (±14)

Table V. Range of thickness averages.

Specimen category	Stress (SD) (MPa) EMAT	PET
Rim blocks	31 (±16)	53 (±22)
As-manufactured	56 (±20)	55 (±19)

From all this, we recommend making several measurements on each specimen and averaging the results. This will reduce the stress uncertainty due to texture variations to about ±50 to 60 MPa.

For field applications, the question is how many points are necessary for an average with an acceptable uncertainty. One measurement may be enough if an uncertainty of about 50 MPa is acceptable. We looked at the effect of averaging three measurements from three equidistant points (about 120° apart) around the circumference. Figure 11 shows that this very limited average is not likely to vary from the average of twenty points by more than ±15 MPa for three random measurements. This seems a very reasonable and acceptable compromise.

Like Fig. 8 for the through-thickness, Fig. 12 shows the spread in near-surface stress measured on individual specimens with the PET. Again, for the as-manufactured and 34 kW conditions, the number of measurements was limited, while there was a full complement for the other power groups. The horizontal tick shows the average in Table III.

By comparing Figs. 12a and b, the difference in front and back rim stresses, noted above, is apparent. On the frf the surface stress decreases rapidly with damage, while on the brf it increases slowly.

For the thickness-averaged stresses, any distinction between the two brake shoe positions was statistically insignificant. Two of the power groups in Fig. 12a, however, do show a possible effect. For all the groups of four, the first two are for centered brakes, and the last two are for flanged brakes. For both 63 kW and 67 kW, these two pairs show a distinction. In both cases, the centered-brake wheels have a lower frf surface stress than the flanged-brake wheels. The distinction is not obvious on the brf. Perhaps there is more heat flow to the frf when the brakes are nearer to this rim (centered).

Figure 13 consolidates further the data in Fig. 12. This shows the average and spread of averages for each power group. Because of the center/flange distinction, the spread is greatest on the frf for 63 kW and 67 kW.

7. DESTRUCTIVE MEASUREMENTS

Saw cutting is a standard quality-control test that gives a global overview of the state of residual bulk hoop stress in the wheel. While not yielding details around the circumference, this procedure is relatively fast and simple. A clip gage on the flange tip measures the amount and direction of movement at the edges of the saw cut as the blade penetrates the rim along a radius

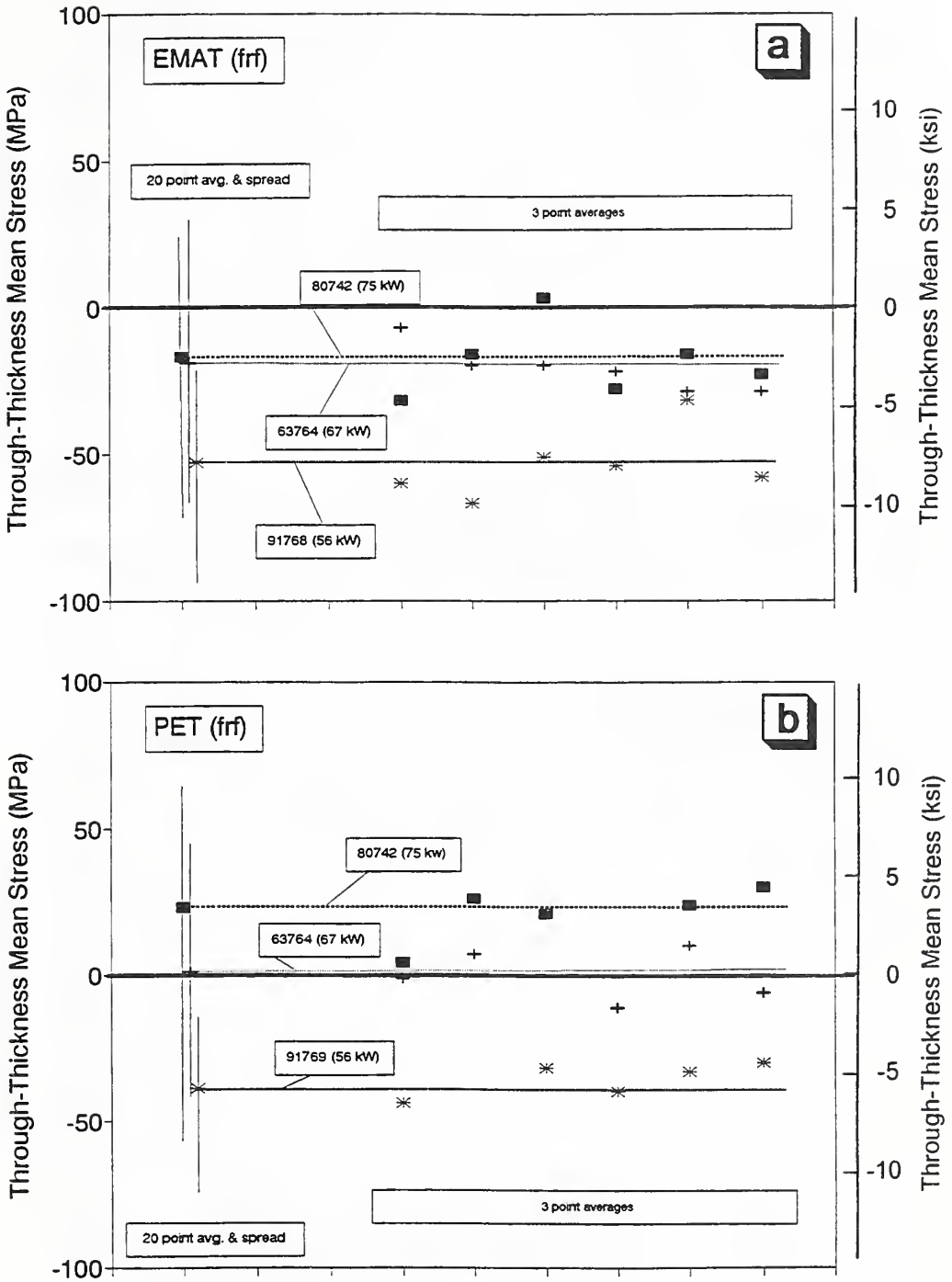

Fig. 11. Comparison of through-thickness average stresses. The horizontal line is the average calculated from all 20 points around the circumference for 3 damaged wheels. The vertical line shows the total spread of all 20 points. The 6 points to the right are averages calculated from just 3 equidistant points.
a. EMAT b. PET

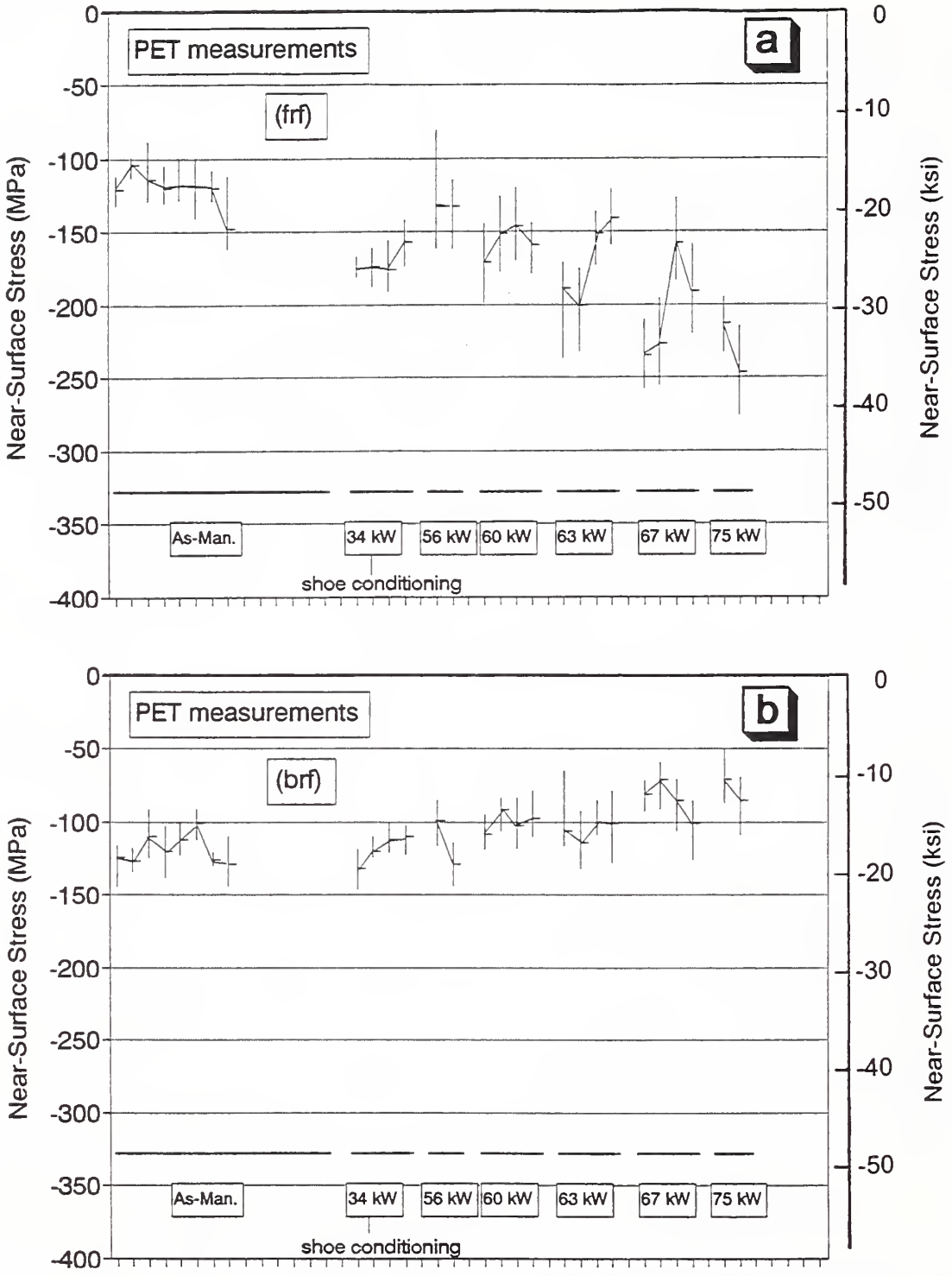

Fig. 12. Spread of near-surface stresses measured with the PET. Each vertical line represents the range for one wheel. The tick on each line shows the average around the circumference. The horizontal bars indicate the power group.
a. frf b. brf

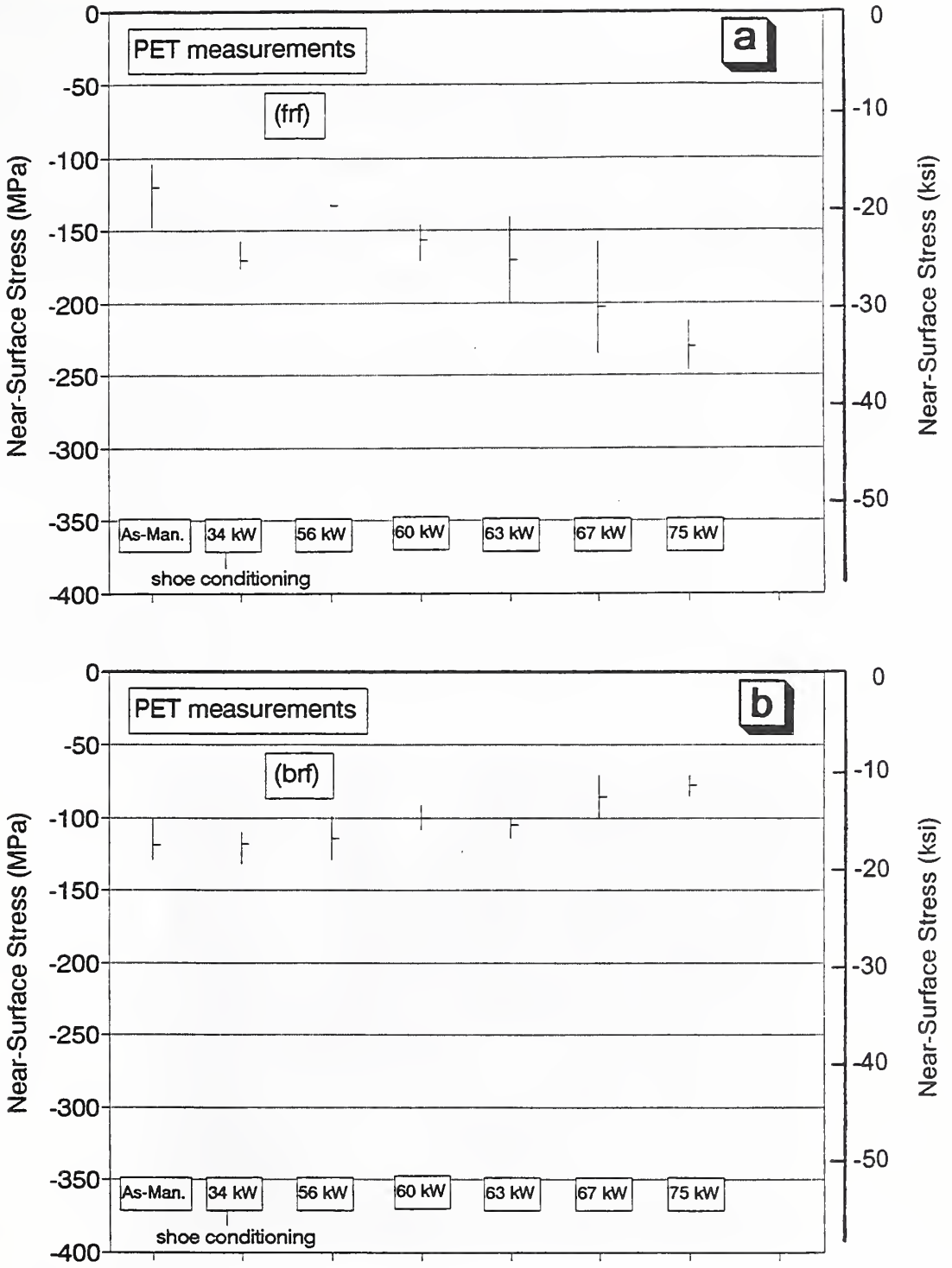

Fig. 13. Spread of the averages in Fig. 12 for each power group. The vertical line shows the total range of the averages and the tick is the average of the averages.
a. frf b. brf

(Fig. 14). Releasing the mechanical restraint relieves the net rim force [23] and this displacement measures the bulk state of stress responsible for crack propagation [30]; qualitatively, slot closure indicates compressive hoop stress and slot opening means tensile stress. At a cut depth of 76 mm (3 in), the local rim forces should be effectively released. Largely due to the restraint of the plate, cuts as deep as 127 mm (5 in) have no noticeable effect on the rim forces only a short distance away (<¼ circumference). For the current specimens, the manufacturer made two cuts on sixteen wheels (Table VI). Two wheels exploded due to tensile forces before the saw cut reached the 76-mm depth. Two other wheels will undergo very detailed DE to analyze stress distributions.

As seen in Table VI, the thermal damage with brake shoes in the flanged position is generally greater than when they are centered. In the 75 kW test, the brake shoes seemed to fail by structural overload or degradation, not by thermal breakdown as in the other tests; this mechanical failure lead to lower heat input and smaller cut openings at 75 kW than at 67 kW.

A qualitative observation during saw cutting was that the saw cut slot was narrower at the frf and wider at the brf. This agrees with the near-surface stresses measured with the PET; after thermal abuse, the stress was compressive on the frf and tensile on the brf. This imbalance in forces would induce out-of-plane bending to account for the observed wedging in the slot.

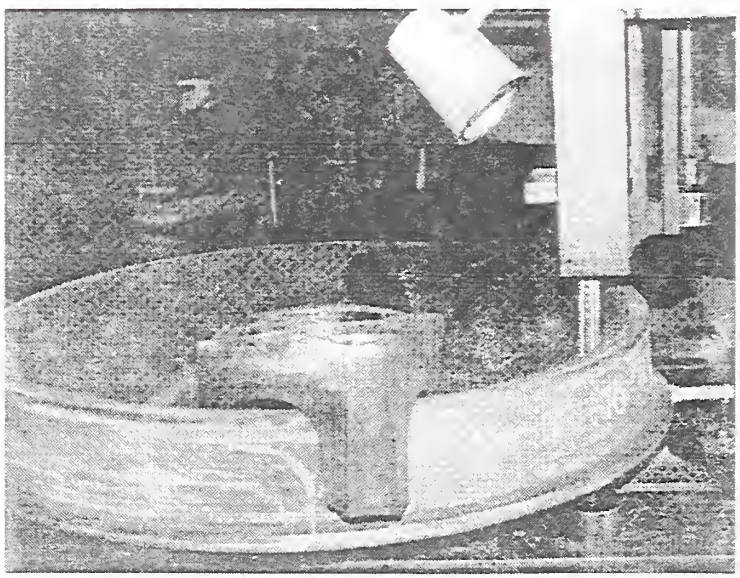

Fig. 14. Destructive evaluation of residual stress by saw cutting. As the saw blade passes through the rim, the clip gage measures the opening or closing of the slot.

Table VI. Saw cut opening when the blade was 76 mm (3 in) deep, just through the rim.

Wheel ID	First cut		Second cut	
	Circum. pos.	Opening (μm)	Circum. pos.	Opening (μm)
91817	9	-76	5	-79
91768	1	-188	5	-191
91843	1	-114	1.5	-104
91807	In progress			
84967	5.5	-18	3	-18
91778	2	+43	6	+20
91777	8.5	-104	2	-64
91784	7	-124	3	-135
91843	1	+23	5	+23
91847	4	+41	10	+51
76933	7.5	+152	3	+97
76896	1.5	+30	7.5	+43
63764	8	+71	8	+51
83991	8.5	+84	3	+71
80742	1	+30	5	0
80582	In progress			
84758	5	+20	1.5	+53
84972	2.5	+185	3	+196
86398	8	explode (~45 mm cut)		
80887	1.5	explode (~45 mm cut)		

8. DATA EVALUATION

Combining the two surface stresses (Table III) and the through-thickness stress (Table II), gives us Fig. 15 as a possible stress distribution through the rim thickness. This is consistent with some previous model calculations [31-34]. While this gives insight into what is happening to the wheel, measuring the surface stress may not be a reliable indicator of overall wheel condition. Parts of the wheel history (e.g., passing through retarders) may affect only the surface condition without causing bulk stresses that might drive crack growth.

The incremental damage curve [30] is a way of collecting the data. As originally presented, it plotted the flange tip saw cut response (at a radial depth of 76 mm, just through the rim) as a function of the input power generating the thermal damage. Figure 16 is a similar curve where the abscissa is the NDE stress change from an average, as-manufactured value, and the ordinate is the clip-gage measurement during DE. Figure 16 combines the data from all of the specimens, even when the power or configuration were different. By calculating the change from an average as-manufactured stress, we hope to minimize variations due to texture.

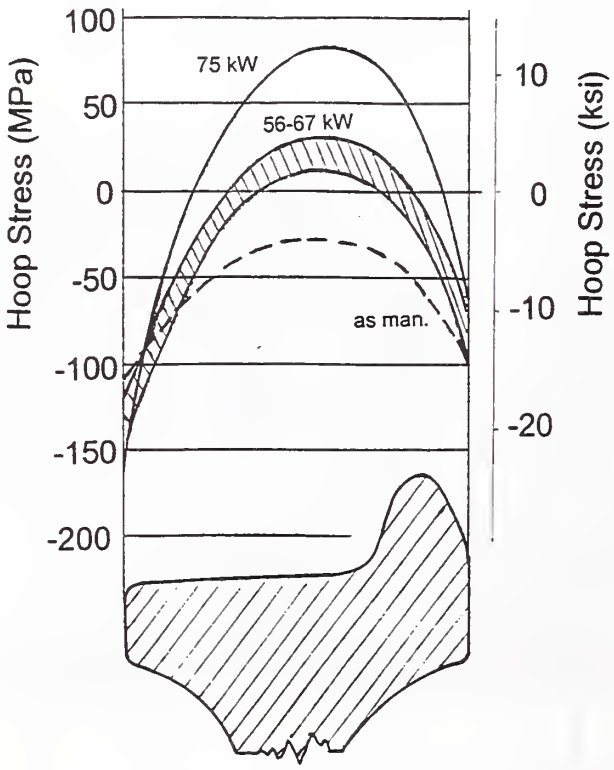

Fig. 15. Suggested stress distribution through the rim thickness for several damage levels, based on stresses at the two rim faces and averaged through the thickness.

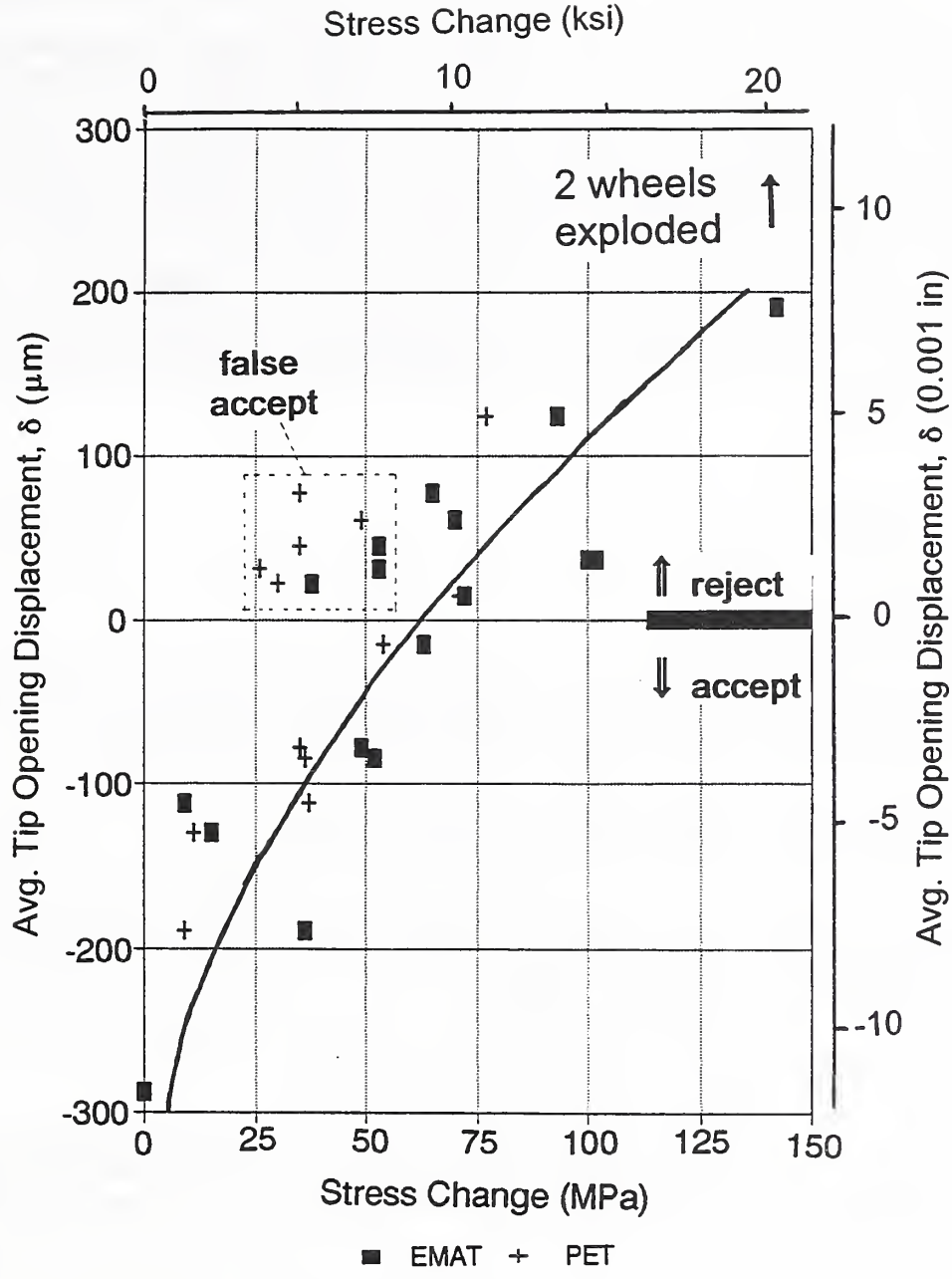

Fig. 16. Incremental damage curve. These data include 16 wheels damaged on a dynamometer. The tip opening displacement is the average of two radial cuts 76 mm deep and the stress is the circumferential average. The change in stress is from the average measured in as-manufactured wheels. We used a tip opening from a prior measurement on a new wheel that was felt to be representative. The choice of zero displacement as the accept/reject boundary is arbitrary and needs refinement.

The curve in Fig. 16 is a simple fit to all the plotted data and will need further refining as additional data become available. For this discussion, we use this curve as an approximation for now, and arbitrarily choose the zero tip-opening displacement (neutral average hoop stress) as the accept/reject criterion. Within this framework, there are eight points from five wheels that would be falsely accepted (the measured stress change projected onto the curve would predict a small saw cut closure when there was actually a small opening). It could be argued that zero displacement is conservative since the openings seen in the two wheels that exploded were far off the scale of Fig. 16 just before fracture at a cut depth of ~45 mm. On the other hand, fracture-mechanics calculations for bridge beams have suggested that cracks may propagate even if the average stress is slightly compressive due to stress redistribution around a crack from a region of tensile stress [35]; if true here, a somewhat negative displacement might be the proper cutoff.

9. CONCLUSIONS

This study has indicated:

1. Acoustoelastic measurements can readily distinguish between wheels with minimal thermal damage and those with potentially dangerous hoop stresses.

2. Measurement repeatability gives confidence to results.

3. With a spread (largely due to texture) of about 50 to 60 MPa, this method should be useful as a screening tool in a maintenance shop since a tensile stress >300 MPa appears to be necessary for spontaneous failure.

4. The correlation between NDE and DE is encouraging.

5. As currently configured, the instrumentation is usable outside the laboratory. Further developments in automation will increase the speed and ease of use even further.

Future work might include:

1. Increased automation [20].

2. Expansion of the data base to in-service wheels.

3. Expanded operation by technicians.

ACKNOWLEDGMENTS

We thank the Federal Railroad Administration for funding this research and our contract monitor, Donald Gray, for considerable guidance. The Association of American Railroads, Transportation Technology Center in Pueblo, Colorado, has provided us with information, insights, and rimblock specimens; we are particularly grateful to Greg Garcia, Robert Florom and Dan Stone. Greg Garcia also collected some NDE measurements. Griffin Wheel Co. and Richard A. Pilon were invaluable in providing our test wheels, damaged on their dynamometer, and supplying the DE data. Julian Deputat of the Institute of Fundamental Technological Research of the Polish Academy of Sciences made possible both the visit of Jacek Szelążek to our laboratory and the use of the DEBRO instrument.

10. REFERENCES

1. J.H. Armstrong, "Keeping Wheels in Shape," Railway Age, Feb. 1985, pp. 39-48.

2. G.L. Marini, "La Rupture des Roues Monobloc - L'Experience des FS," *Proceedings, Eleventh International Wheelset Congress*, Vol. 2, Paris, June 1995, pp. 87-93.

3. K. Osuch, D.H. Stone, and O. Orringer,"European and American Wheels and their Resistance to Thermal Damage," *Proceedings, Eleventh International Wheelset Congress*, Vol. 1, Paris, June 1995, pp. 77-86.

4. M.T. Gallagher and C.D. Christie, "The Influence of Wheel Geometry on the Development of Residual Stress and Rim Deflection," *Proceedings, Eleventh International Wheelset Congress*, Vol. 1, Paris, June 1995, pp. 21-27.

5. Federal Railroad Administration, U.S. Dept. of Transportation, Code of Federal Regulations 49 CFR, 65, §215.03(h), 1985.

6. Office of Research and Development of the Association of American Railroads, *Wheel Failure Mechanisms of Railroad Cars*, Report TFR 53-82-C-00282, 1986.

7. J.R. Barton, W.D. Perry, R.K. Swanson, G.C. Hsu, and S.R. Ditmeyer, "Heat-Discolored Wheels: Safe to Reuse?" Progressive Railroading, Mar. 1985, pp. 41-48.

8. K.-O. Edel, H. Hintze, and M. Korn, "Analysis of a Solid Railway Wheel Breakage," *Rail International*, Jan. 1992, pp. 28-40.

9. H.P. Klug and L.E. Alexander, "Stress Measurement in Metals," *X-Ray Diffraction Procedures*, 2nd edition (John Wiley & Sons, NY, 1974), pp. 755-790.

10. J.H. Root, T.M. Holden, R.J. Klassen, C. Smallman, B. Maxfield, and N.R. Gore, "Neutron Diffraction Measurements of Residual Stress in Rails," *Rail Quality and Maintenance for Modern Railway Operation*, J.J. Kalker, D.F. Cannon, and O. Orringer, eds. (Kluwer Academic Publishers, Boston, 1993), pp. 315-324.

11. D.J. Buttle, W. Dalzell, C.B. Scruby, and R.A. Langman, "Comparison of Three Magnetic Techniques for Biaxial Stress Measurement," *Review of Progress in Quantitative Nondestructive Evaluation*, Vol. 9B, D. O. Thompson and D. E. Chimenti, eds. (Plenum Press, NY, 1990), pp. 1879-1885.

12. R.R. King, J.A. Birdwell, D.E. Bray, W.N. Clorfelter, and E.R. Risch, "Improved Methods for Nondestructively Measuring Residual Stress in Railway Wheels," *Proceedings, Ninth Symposium on NDE*, San Antonio, Texas, April 25-27, 1973, pp. 91-105.

13. G.A. Matzkanin, R.E. Beissner, and C.M. Teller, *The Barkhausen Effect and its Applications to Nondestructive Evaluation*, Southwest Research Institute, NTIAC Report 79-2, 1979.

14. H.C. Iwand, "A Comparative Analysis Using Barkhausen Noise Analysis Ultrasonic Birefringence, and Saw Cutting Techniques in Determination of Residual Stress in Railroad Wheels," Thesis, University of Nebraska, Lincoln, 1988.

15. D. Utrata and M. Namkung, "Assessment of the Magnetoacoustic Method for Residual Stress Detection in Railroad Wheels." *Review of Progress in Quantitative Nondestructive Evaluation*, Vol. 12B, D.O. Thompson and D.E. Chimenti, eds. (Plenum Press, NY, 1993), pp. 1807-1814.

16. H. Häusler, G. König, and H. Kockelmann,"On the Accuracy of Determining the Variation with Depth of Residual Stresses by Means of the Hole-Drilling Method," *Residual Stresses in Science and Technology*, Vol. 1, E. Macherauch and V. Hauk, eds. (DGM Informationgesellschaft mbH, Oberursel, Germany, 1987), pp. 257-264.

17. Y.-H. Pao, W. Sachse, and H. Fukuoka, "Acoustoelasticity and Ultrasonic Measurements of Residual Stresses," *Physical Acoustics*, Vol. XVII, W.P. Mason and R.N. Thurston, eds. (Academic Press, NY, 1984), pp. 61-143.

18. K. Okada, "Stress-Acoustic Relations for Stress Measurement by Ultrasonic Technique," Journal of the Acoustical Society of Japan (E) 1(3): 193-200, 1980.

19. H. Fukuoka, H. Toda, K. Hirakawa, H. Sakamoto, and Y. Toya, "Acoustoelastic Measurements of Residual Stresses in the Rim of Railroad Wheels," *Wave Propagation in Inhomogeneous Media and Ultrasonic Nondestructive Evaluation*, Vol. 6, G. C. Johnson, ed., (ASME, NY, 1984), pp. 185-193.

20. A. Bartosiewicz, A. Brokowski, J. Deputat, K. Mizerski, and J. Szelążek, "Miniature Ultrasonic Stress Gauge for In-Service Inspection of Thermally Damaged Wheels," *Proceedings, Eleventh International Wheelset Congress*, Vol. 1, Paris, June, 1995, pp. 241-246.

21. V. Del Fabbro and B. Catot, "Ultrasonic Measurement of Stresses in New Wheels," *Proceedings, Eleventh International Wheelset Congress*, Vol. 1, Paris, June, 1995, pp. 251-259.

22. R.E. Schramm, A.V. Clark, and J. Szelążek, "Safety Assessment of Railroad Wheels by Residual Stress Measurements," in *Nondestructive Evaluation of Aging Railroads*, Donald E. Gray, Daniel Stone, eds., Proc. SPIE 2458, 97-108 (1995).

23. R. E. Schramm, J. Szelążek, and A.V. Clark, Jr., "Report No. 28 - Residual Stress in Induction-Heated Railroad Wheels: Ultrasonic and Saw Cut Measurements," NISTIR 5038, May 1995.

24. R.E. Schramm, A.V. Clark, Jr., D.V. Mitraković, S.R. Schaps, and T.J. McGuire, "Report No. 23 - Residual Stress Detection in Railroad Wheels: An Ultrasonic System Using EMATs," NISTIR 3968, National Institute of Standards and Technology, 1991.

25. J.C. Tourrade, P.E. Gautier, and B. Catot, "The History of a 515,3 km/hour World Record Wheel," *Proceedings, Tenth International Wheelset Congress*, National Conference Publication (The Institution of Engineers, Australia, Sydney, 1992), pp. 303-310.

26. S.A. Perfect, "Stress Changes in Railroad Car Wheels Due to Axially Symmetric Thermal Loads," Thesis, University of Illinois at Urbana-Champaign, 1986.

27. DEBRO Ultrasonic Stress Meter, Institute of Fundamental Technological Research, Polish Academy of Sciences, Warsaw, Poland, 1990.

28. E. Schneider, R. Herzer, D. Bruche, and H. Frotscher, "Reliability Assurance of Railroad Wheels by Ultrasonic Stress Analysis," *Third European Conference on Residual Stresses*, Nov. 4-6, 1992, Frankfurt, Germany.

29. M. Gori, "Development and Qualification of an Ultrasonic Method for the Evaluation of Residual Stress in the Rim of Railroad Wheels," CISE SpA - DSD/SME, Via Reggio Emilia 39, 20090 Segrate, C.P. 12081-I, 20134 Milano, Italy.

30. M.T. Gallagher and M.A. Polzin, "Defining the Thermal Tolerance of Curved Plate Heat Treated Wheels," *Proceedings, Tenth International Wheelset Congress*, National Conference Publication (The Institution of Engineers, Australia, Sydney, 1992), pp. 33-38.

31. M.R. Johnson, R.E. Welch, and K.S. Yeung, "Analysis of Thermal Stresses and Residual Stress Changes in Railroad Wheels Caused by Severe Drag Braking," *J. Eng. Ind.*, Vol. 99(1), 1977, pp. 18-23.

32. A.J. Opinsky and M.W. Joerms, "Modeling the Drag Braking of Freight Car Wheels Having a Simulated Heat Treatment," *Proceedings ASME/IEEE Railroad Conference*, V. T. Hawthorne and T. Kneschke, eds. (American Society of Mechanical Engineers, NY, 1988), pp. 37-42.

33. D. Utrata, "Magnetoacoustic Testing of Railroad Wheels: Assessing the Laboratory to Component Test Transition," *Nondestr. Test. Eval.*, Vol. 10, 1992, pp. 81-96.

34. J.E. Gordon, "Simulation of the Quenching Process of Railroad Wheels," *Proceedings, Eleventh International Wheelset Congress*, Vol. 2, Paris, June, 1995, pp. 83-86.

35. T.L. Anderson and A.V. Clark,"New Approaches to Life Assessment of Steel Bridges," to be published as a NISTIR.